Supplementary materials for

Cr(VI) reduction, electricity production, and microbial resistance variation in paddy soil under microbial fuel cell operation

Sections

Section 1: Preparation of cathode supported by Fe_3O_4 catalyst

Section 2: Python code of Raspberry Pi voltage acquisition system

Table Captions

Table S1. Main material dimensions

Table S2. Primer sequence of HRGs and MGEs

Table S3. Distribution percentage of EDS elements in electrode materials

Table S4. SMFC power generation performance on 15-day and 30-day

Table S5. Performance comparison of various conFig.urations of SMFC.

Figure captions

Fig. S1 SMFC structure and experimental grouping.

Fig. S2 Electrode material characterization. (A, B) SEM images of GF without catalyst loading; (C, D) SEM images of aluminum foam.

Fig. S3 Variation of (A) total chromium and (B) Cr(VI) in overlying water during SMFC operation.

Fig. S4 pH (A), EC (B) variation curves of soil.

Fig. S5 Changes in soil enzyme activities during SMFC operation (A) Dehydrogenase (B) Urease (C) Invertase (D) Acid Phosphatase.

Fig. S6 Venn diagram on OTU level in different treatments.

Fig. S7 Characterization of electrode materials before and after operation by EDS mapping. (A) EDS image of cathode loaded with Fe_3O_4; (B) EDS image of cathode after the SMFC operation; (C) EDS image of anode microorganisms; (D) EDS image of the anode after SMFC operation.

Section 1: Preparation of cathode supported by Fe_3O_4 catalyst

Cathode preparation: 100×50×3 mm graphite felt (GF) (purchased from Jiangsu Xinye Electronic Materials Factory, Jjiangsu, China) was selected as the cathode material of the SMFC, which was ultrasonicated in ethanol for 50 min to remove impurities, removed, and washed. Then put it into an oven and dried at 60℃ for 12 h. It was put into the hydrothermal synthesis reactor and added concentrated nitric acid, and reacted at 90℃ for 9 h. After the reaction was completed, the GF was rinsed continuously with ultrapure water to ensure that the pH of the rinsed water was neutral, and dried at 60℃ for 12 h to complete the pre-activation of the GF. The Fe_3O_4 catalyst was obtained by dissolving 3.6 g of ferric chloride hexahydrate, 6 g of sodium acetate, and 1 g of sodium citrate in 140 ml of ethylene glycol, and repeatedly ultrasonicating for 2 h to form a homogeneous solution. The pre-activated GF was put into a hydrothermal synthesis reactor: the Fe_3O_4 catalyst was added and soaked for half an

hour and then heated at 200℃ for 8 h. After heating, the reactor was cooled down to room temperature, washed repeatedly with ultrapure water and ethanol, and then put into an oven at 60℃ to dry for 12 h. The reaction was then dried at 60℃.

Section 2: Python code of Raspberry Pi voltage acquisition system

```
# -*- coding:UTF-8 -*-
from threading import Timer
import time
import RPi.GPIO as GPIO
import datetime
import os
import sys
import xlwt

sys.path.append('./modules/')

from GetVoltage import get_voltage
from modules.ADS1263 import ADS1263

GPIO.setmode(GPIO.BCM)
CollectTimes = 150

def _get_average_list():
    """smooth"""
    if CollectTimes <= 0:
        print("Error number for the array to averaging!/n")
        return -1
    elif CollectTimes <= 5:
        return sum(VoltageArray) / CollectTimes
    else:
        return sum(VoltageArray) / CollectTimes

# clean txt
book = xlwt.Workbook(encoding='utf-8',style_compression=0)
sheet = book.add_sheet('MFCdata',cell_overwrite_ok=True)
col = ('current time','MFC1','MFC2','MFC3')
for i in range(0,4):
    sheet.write(0,i,col[i])

x=0
while(1):
    x=x+1

    time.sleep(1)

```

```
41.     VoltageArray = []
42.     for i in range(CollectTimes):
43.         VoltageArray.append(get_voltage(0))
44.     adc1 = _get_average_list()
45.
46.     ##########################################################
47.
48.     VoltageArray = []
49.     for i in range(CollectTimes):
50.         VoltageArray.append(get_voltage(1))
51.     adc2 = _get_average_list()
52.
53.     ##########################################################
54.
55.     VoltageArray = []
56.     for i in range(CollectTimes):
57.         VoltageArray.append(get_voltage(2))
58.     adc3 = _get_average_list()
59.
60.     ##########################################################
61.
62.     curr_time = datetime.datetime.now()
63.     time_str = datetime.datetime.strftime(curr_time,'%Y-%m-%d %H:%M:%S')
64.
65.     datalist = [time_str,str(adc1),str(adc2),str(adc3 )]
66.     print(datalist)
67.
68.     for j in range(0, 4):
69.         sheet.write(x, j, datalist[j])
70.         savepath = '/home/pi/excel.xls'
71.         book.save(savepath)
72.
73.     time.sleep(598.5)
```

Table S1 Main material dimensions

Material	Length/cm	Width/cm	Area/cm^2
Collector plate	10.5	5.5	57.75
Aluminum foam	6.6	5.4	35.64
GF	10.0	5.0	50.00

Table S2 Primer sequence of HRGs and MGEs

Gene	Primer sequence	Function description	Ref
chrA-F	TCC TTC GGC GGC CCT GCCggncarathgc	*chrA* encodes a transporter protein involved in chromate efflux.	(Rivera et al., 2008)
chrA-R	GTA GGT GGC CAG CTG Ctngcytcnggncc		
chrB-F	CCGGAATTCATGCGTGTCTGGCGAACCCTGA	*chrB* genes regulate the transcription of genes in the transporter protein complex.	(Branco and Morais, 2013)
chrB-R	CCC AAG CTT TCA CTC TGC GGA AGA ACG A		
ChrR-F	AGG AAC TTC TGC GTG CCC TC	The chromate reductase chrR is the best-known of the reductases that catalyze the reduction of Cr^{6+} to Cr^{3+}.	(Baldiris et al., 2018; Nepple et al., 2000).
ChrR-R	TAC GGT GAC AGT GCG TTT GC		
IntI-F	CGA ACG AGT GGC GGA GGG TG	MGEs such as integrons, plasmids, and transposons play a key role in the transfer of resistance genes between different microorganisms in the environment	(Wu et al., 2023; Wu et al., 2022).
IntI-R	TAC CCG AGA GCT TGG CAC CCA		
tnpA02-F	GGG CGG GTC GAT TGA AA		
tnpA02-R	GTG GGC GGG ATC TGC TT		
tnpA05-F	GCC GCA CTG TCG ATT TTT ATC		
tnpA05-R	GCG GGA TCT GCC ACT TCT T		

Table S3 Distribution percentage of EDS elements in electrode materials.

Elements	Samples					
	Cathode	Fe_3O_4-cathode	Cathode after operation	Anode	Anode with EAB-loading	Anode after operation
C	93.74%	66.85%	33.83%	6.7%	14.65%	14.35%
O	6.26%	19.97%	38.96%	47.57%	18.49%	50.92%
Fe	n.d.	13.17%	8.07%	n.d.	n.d.	0.88
Mg	n.d.	n.d.	0.44%	n.d.	0.41%	n.d.
Al	n.d.	n.d.	3.34%	37.04%	53.72%	17.56%
Cr	n.d.	n.d.	0.08%	n.d.	n.d.	0.12%
Cu	n.d.	n.d.	n.d.	n.d.	1.59%	n.d.
Zn	n.d.	n.d.	n.d.	n.d.	1.81%	n.d.
Si	n.d.	n.d.	7.16%	8.68%	9.32%	2.58%
Na	n.d.	n.d.	2.18%	n.d.	n.d.	4.55%
Ca	n.d.	n.d.	4.81%	n.d.	n.d.	n.d.
K	n.d.	n.d.	1.12%	n.d.	n.d.	0.58%
Cl	n.d.	n.d.	n.d.	n.d.	n.d.	2.67%
P	n.d.	n.d.	n.d.	n.d.	n.d.	5.81%

Table S4 SMFC power generation performance on 15-day and 30-day

Resistor (Ω)	15d-Current density (mA/m^2)	15d-Power density (mW/m^2)	30d-Current density (mA/m^2)	30d-Power density (mW/m^2)
51	448.57	37.43	485.23	42.21
100	386.53	53.84	424.57	63.47
200	296.55	62.24	357.26	90.22
510	202.88	73.52	238.08	102.02
1000	131.18	60.60	157.54	87.35
2000	75.99	40.43	95.91	64.58
5100	31.55	17.77	43.88	34.41

10000	17.01	10.13	23.95	20.09

Table S5 Performance comparison of various conFig.urations of SMFC.

Reactor conFig.uration	Chamber volume (L)	Output voltage （V）	Maximum power density (mW/m^2)	Reference
Single-chamber SMFC	0.72	0.33	17.3	(Li et al., 2016)
Single-chamber SMFC	2.16	0.297	12.1	(Yu et al., 2017)
Two-chamber SMFC	4.2	0.399	29.78	(Srivastava et al., 2019)
Single-chamber circle SMFC	0.95	0.345	24	(Yu et al., 2021)
Single-chamber SMFC	8	0.4-0.6	0.2 mW	(Yoon et al., 2023)
Single-chamber circle SMFC	n.m.	n.m.	25.51	(Wang et al., 2023)
Single-chamber SMFC	9.7	n.m.	70.4±1.4	(Dhillon et al., 2023)
Two-chamber SMFC	0.05	n.m.	71.00 ± 0.82	(Zhang et al., 2023a)
Constructed wetland MFC	38.85	0.197	12.5	(Tao et al., 2023)
Constructed wetland MFC	4.08	0.425	28.1	(Niu et al., 2023)
Plant-SMFC	0.769	0.51	46.8	(V et al., 2023)
Single-chamber circle SMFC	2	0.17	10	(Youssef et al., 2023)
Constructed wetland MFC	2.7	0.394	4468.4	(Zhang et al., 2023b)
Two-chamber SMFC	0.5	0.306	20.35	(Zhang et al., 2024)
Constructed wetland MFC	13	0.167	1.4	(Dai et al., 2024)
Plant-SMFC	1.05	0.55	8957.7	(Chen et al., 2024)
Single-chamber circle SMFC	1.6	0.4	472.52±14.2	(Zhao et al., 2024)
Single-chamber	1.4	0.528	178.17	(Sun and Wang,

circle SMFC				2024)
Single-chamber SMFC	2.3	0.75	102	This study

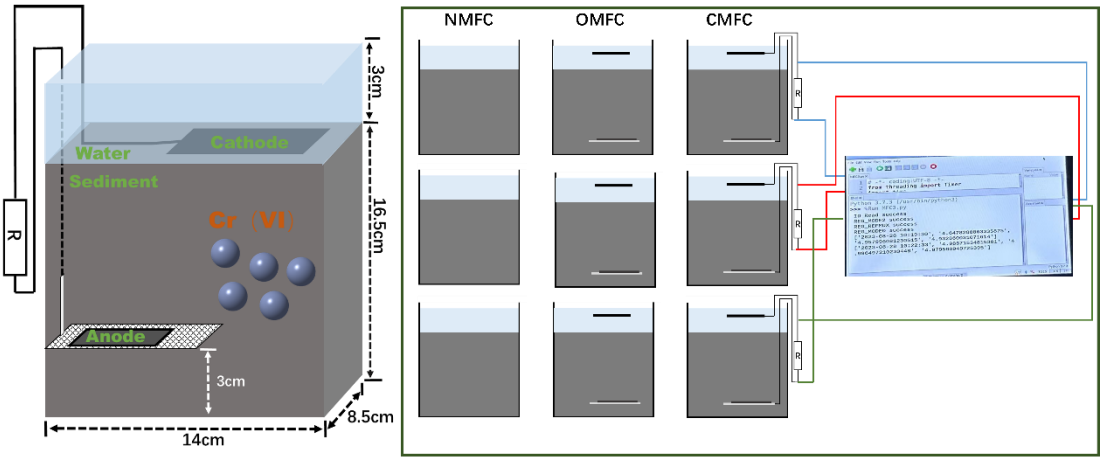

Fig. S1 SMFC structure and experimental grouping.

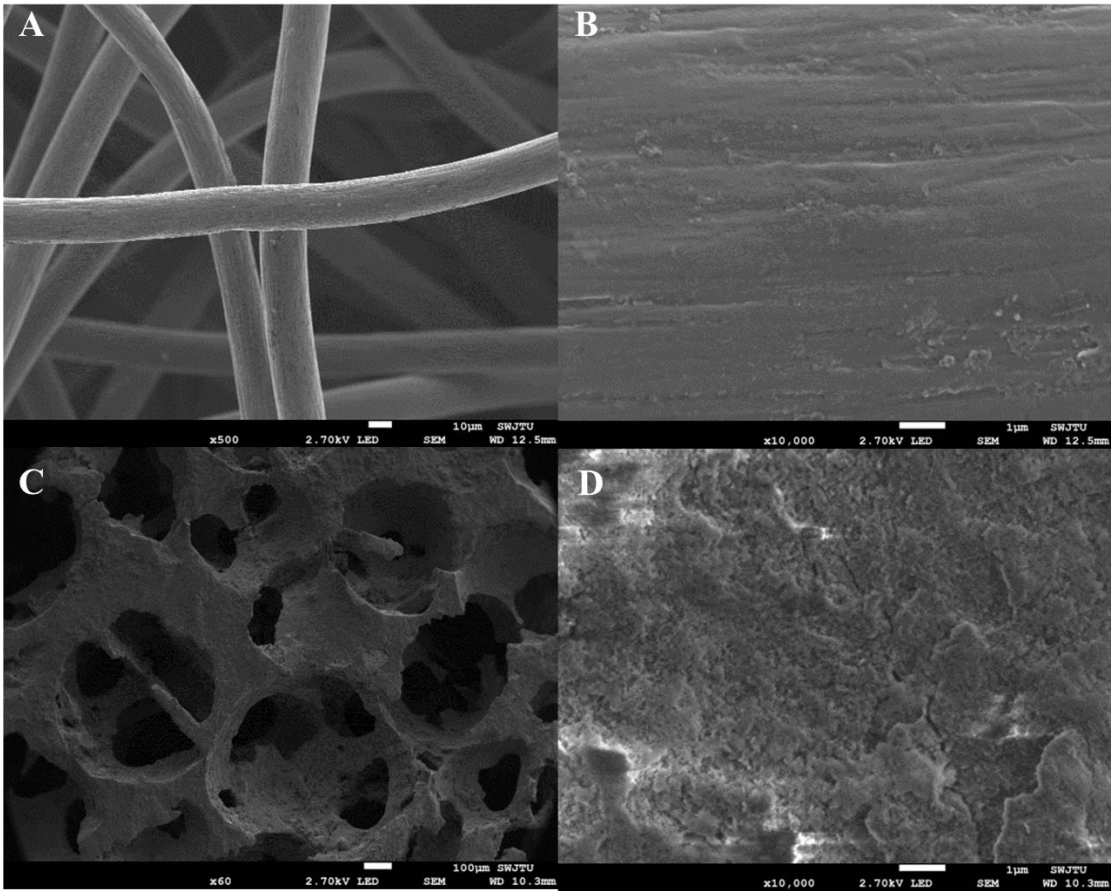

Fig. S2 Electrode material characterization. (A, B) SEM images of GF without

catalyst loading; (C, D) SEM images of aluminum foam.

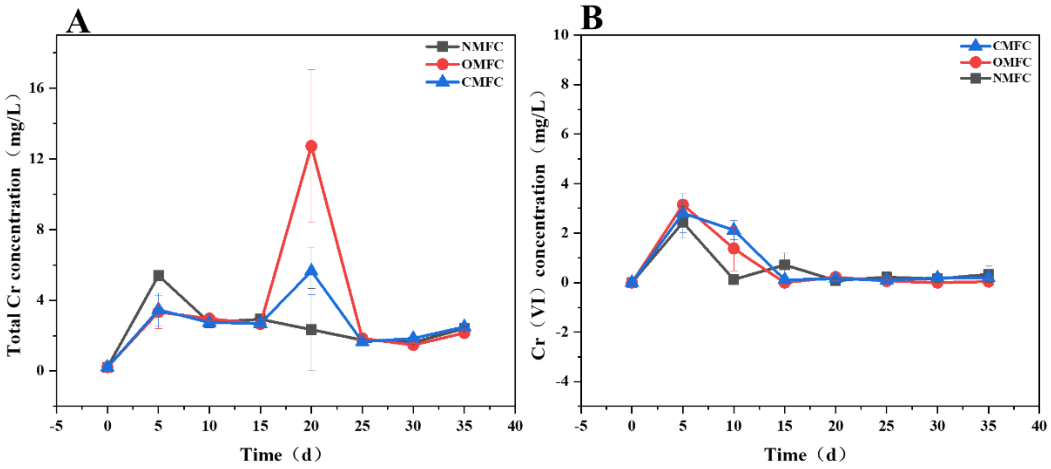

Fig. S3 Variation of (A) total chromium and (B) Cr(VI) in overlying water during SMFC operation.

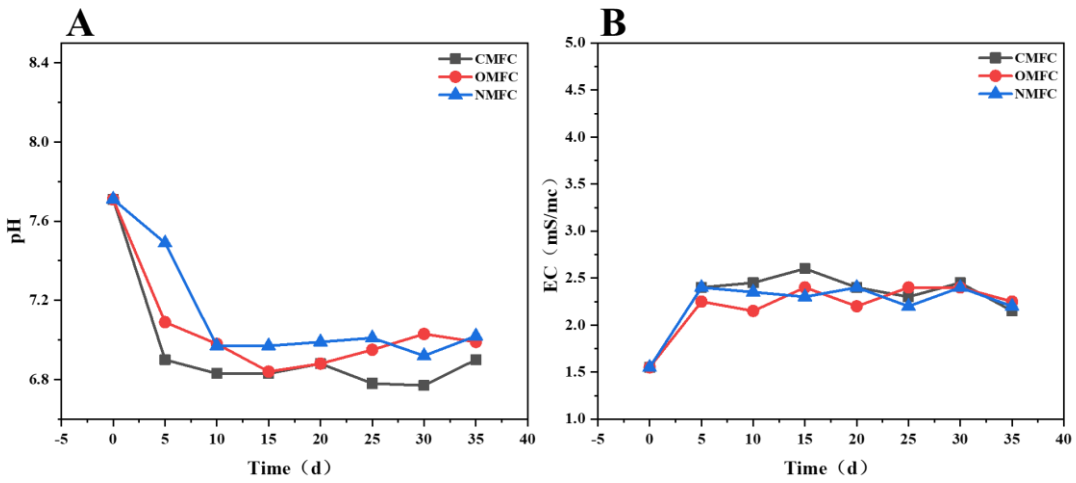

Fig. S4 pH (A), EC (B) variation curves of soil.

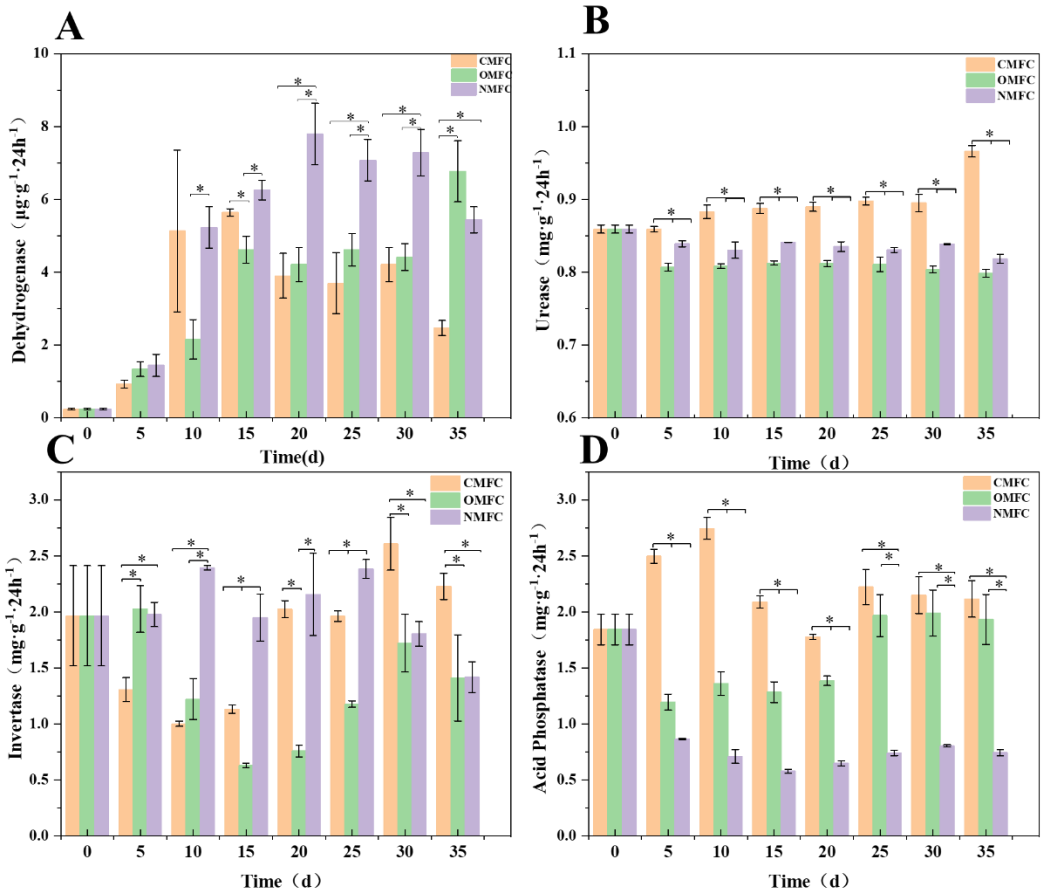

Fig. S5 Changes in soil enzyme activities during SMFC operation (A) Dehydrogenase (B) Urease (C) Invertase(D) Acid Phosphatase.

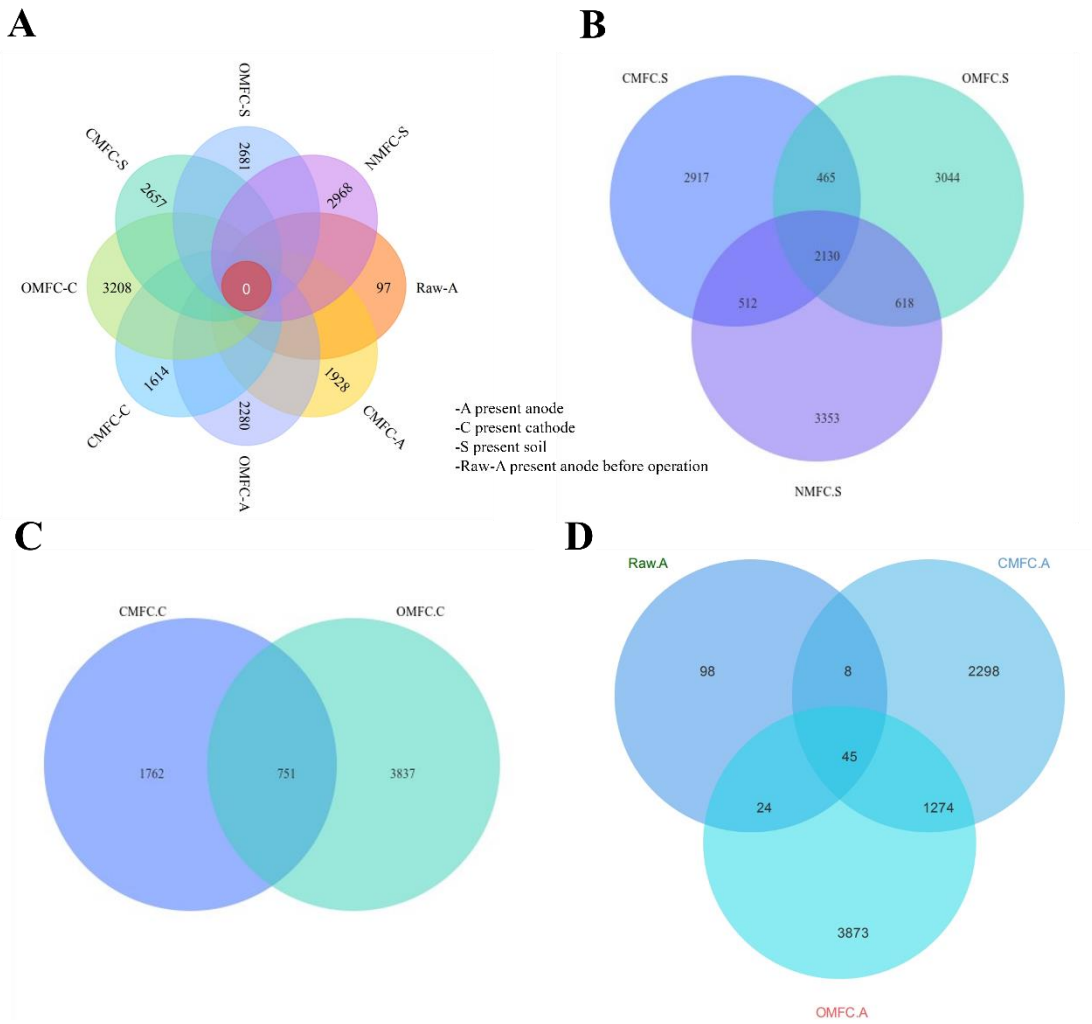

Fig. S6 Venn diagram on OTU level in different treatments

A

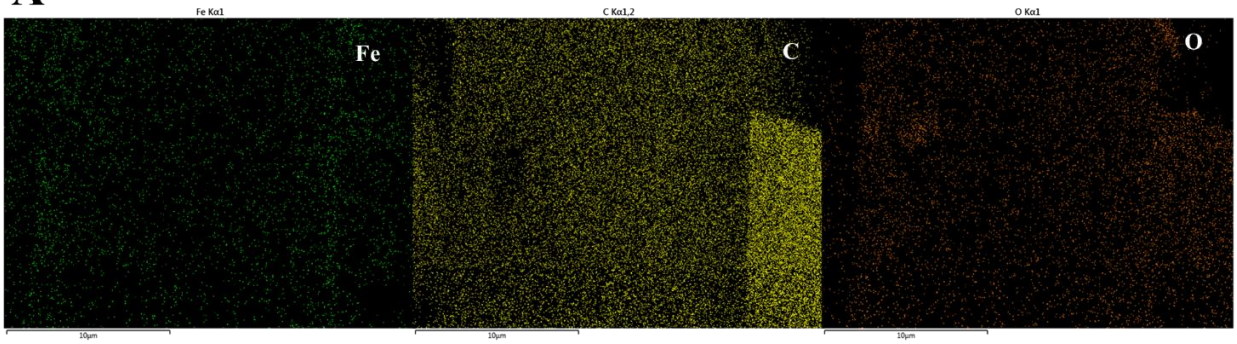

B

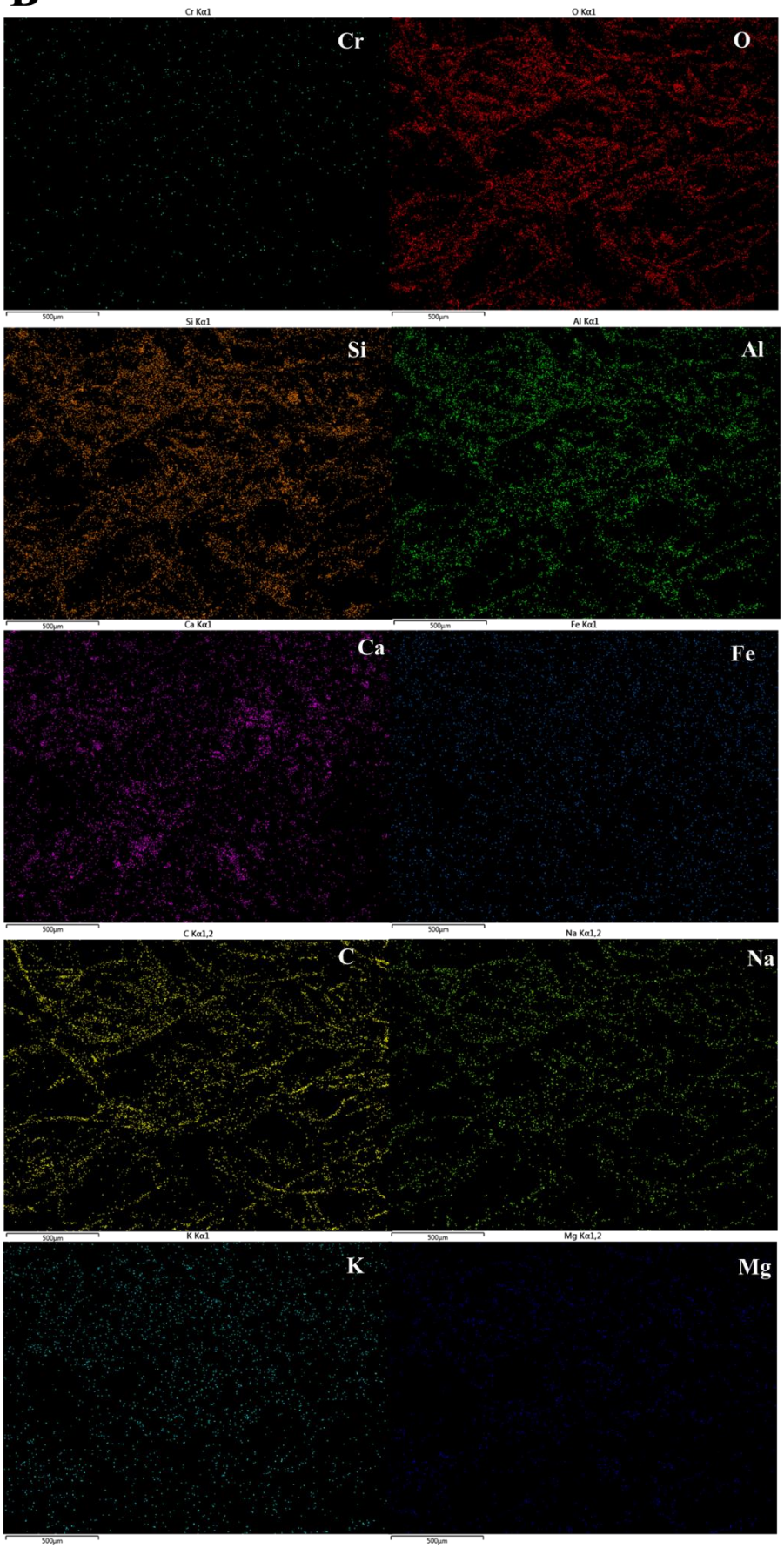
Cr Kα1
Cr
O Kα1
O
500μm
500μm
Si Kα1
Si
Al Kα1
Al
500μm
500μm
Ca Kα1
Ca
Fe Kα1
Fe
500μm
500μm
C Kα1,2
C
Na Kα1,2
Na
500μm
500μm
K Kα1
K
Mg Kα1,2
Mg
500μm
500μm

C

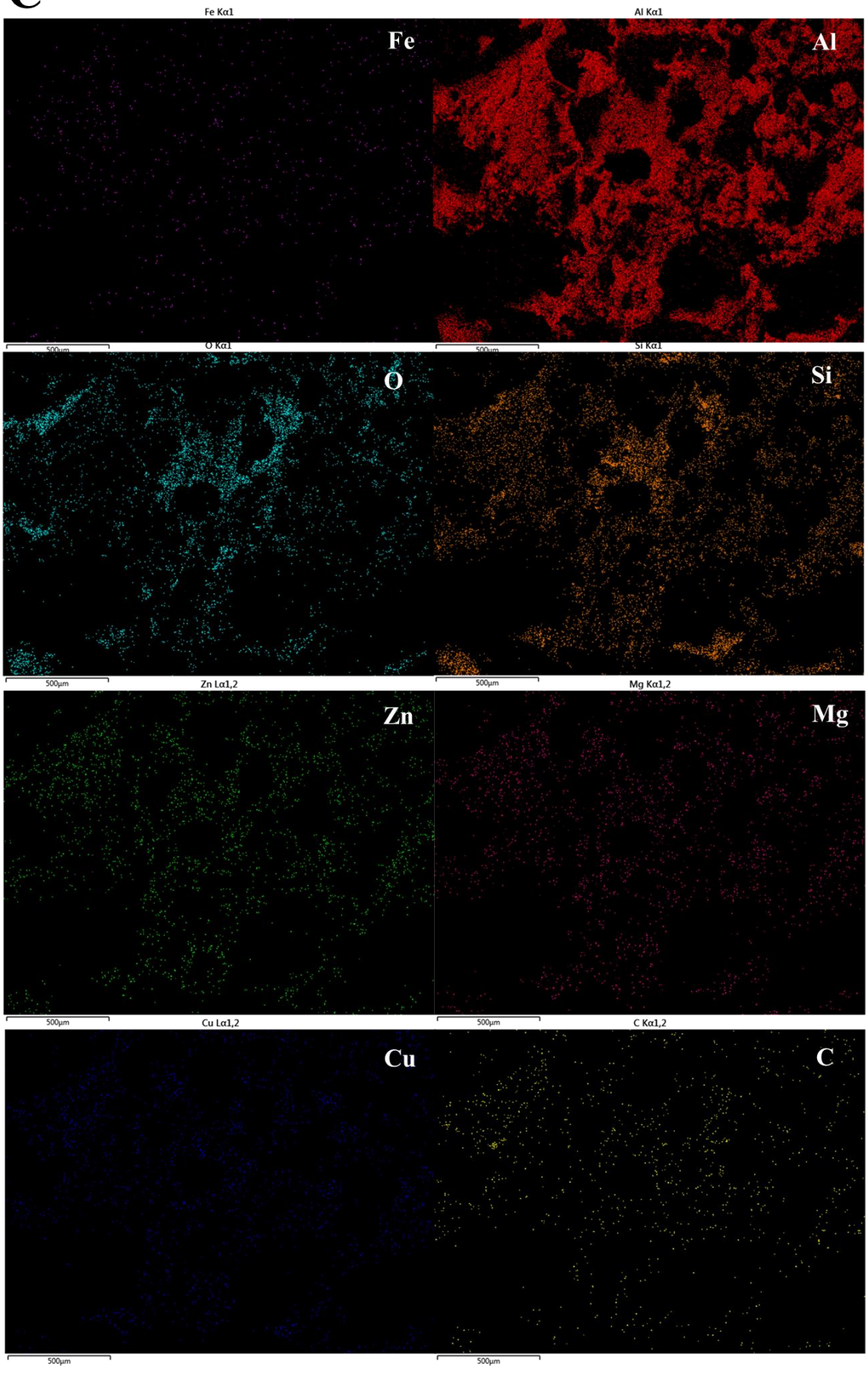
Fe Kα1
Fe
Al Kα1
Al
500μm
500μm
O Kα1
O
Si Kα1
Si
500μm
500μm
Zn Lα1,2
Zn
Mg Kα1,2
Mg
500μm
500μm
Cu Lα1,2
Cu
C Kα1,2
C
500μm
500μm

D

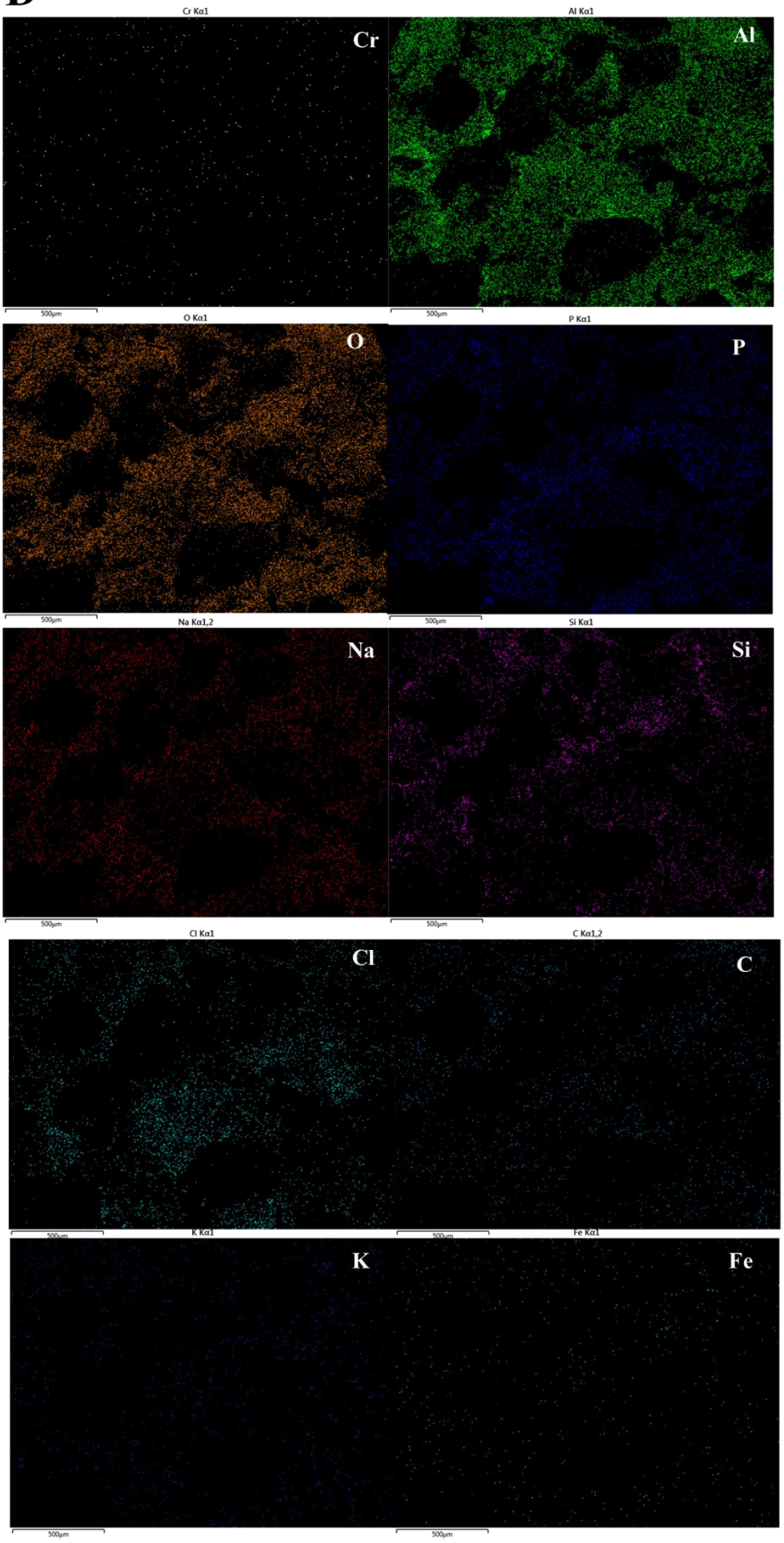
Cr Kα1
Cr
Al Kα1
Al
500μm
O Kα1
O
P Kα1
P
Na Kα1,2
Na
Si Kα1
Si
Cl Kα1
Cl
C Kα1,2
C
K Kα1
K
Fe Kα1
Fe

Fig. S7 Characterization of electrode materials before and after operation by EDS mapping. (A) EDS image of cathode loaded with Fe_3O_4; (B) EDS image of cathode after the SMFC operation; (C) EDS image of anode microorganisms; (D) EDS image of the anode after SMFC operation.

Reference:

Baldiris, R., Acosta-Tapia, N., Montes, A., Hernández, J., Vivas-Reyes, R., (2018). Reduction of Hexavalent Chromium and Detection of *Chromate Reductase* (*ChrR*) in *Stenotrophomonas maltophilia*. Molecules 23(2), 406. https://doi.org/10.3390/molecules23020406.

Branco, R., Morais, P.V., (2013). Identification and Characterization of the Transcriptional Regulator ChrB in the Chromate Resistance Determinant of Ochrobactrum tritici 5bvl1. PLoS One 8(11), e77987. https://doi.org/10.1371/journal.pone.0077987.

Chen, B., Li, L., Cai, W., Garg, A., (2024). Bioelectricity generation in plant microbial fuel cells: Influence of vegetation density and unsaturated soil properties. Biomass and Bioenergy 181, 107053. https://doi.org/10.1016/j.biombioe.2024.107053.

Dai, M., Li, F., Zhang, J., Shi, Q., Wu, Y., Kong, Q., (2024). Treatment of formaldehyde-containing wastewater and power generation by constructed wetland–microbial fuel cells enhanced by formaldehyde-degrading bacteria. Journal of Water Process Engineering 59, 104984. https://doi.org/10.1016/j.jwpe.2024.104984.

Dhillon, S.K., Dziegielowski, J., Kundu, P.P., Di Lorenzo, M., (2023). Functionalised graphite felt anodes for enhanced power generation in membrane-less soil microbial fuel cells. RSC Sustainability 1(2), 310-325. https://doi.org/10.1039/D2SU00079B.

Li, X., Wang, X., Zhao, Q., Wan, L., Li, Y., Zhou, Q., (2016). Carbon fiber enhanced bioelectricity generation in soil microbial fuel cells. Biosensors and Bioelectronics 85, 135-141. https://doi.org/10.1016/j.bios.2016.05.001.

Nepple, B.B., Kessi, J., Bachofen, R., (2000). Chromate reduction by *Rhodobacter sphaeroides*. Journal of Industrial Microbiology and Biotechnology 25(4), 198-203. https://doi.org/10.1038/sj.jim.7000049.

Niu, Y., Qu, M., Du, J., Wang, X., Yuan, S., Zhang, L., Zhao, J., Jin, B., Wu, H., Wu, S., Cao, X., Pang, L., (2023). Effects of multiple key factors on the performance of petroleum coke-based constructed wetland-microbial fuel cell. Chemosphere 315, 137780. https://doi.org/10.1016/j.chemosphere.2023.137780.

Rivera, S.L., Vargas, E., Ramírez-Díaz, M.I., Campos-García, J., Cervantes, C., (2008). Genes related to chromate resistance by *Pseudomonas aeruginosa PAO1*. Antonie Van Leeuwenhoek 94(2), 299-305. https://doi.org/10.1007/s10482-008-9247-x.

Srivastava, P., Gupta, S., Garaniya, V., Abbassi, R., Yadav, A.K., (2019). Up to 399 mV bioelectricity generated by a rice paddy-planted microbial fuel cell assisted with a blue-green algal cathode. Environmental Chemistry Letters 17(2), 1045-1051. https://doi.org/10.1007/s10311-018-00824-2.

Sun, M., Wang, C., (2024). The application of ferrous and graphitic N modified graphene-based composite cathode material in the bio-electro-Fenton system

driven by sediment microbial fuel cells to degrade methyl orange. Heliyon 10(3), e24772. https://doi.org/10.1016/j.heliyon.2024.e24772.

Tao, M., Kong, Y., Jing, Z., Guan, L., Jia, Q., Shen, Y., Hu, M., Li, Y.-Y., (2023). Acorus calamus recycled as an additional carbon source in a microbial fuel cell-constructed wetland for enhanced nitrogen removal. Bioresource Technology 384, 129324. https://doi.org/10.1016/j.biortech.2023.129324.

V, K.K., K, M.m., Manju, P., Gajalakshmi, S., (2023). Harnessing plant microbial fuel cells for resource recovery and methane emission reduction in paddy cultivation. Energy Conversion and Management 294, 117545. https://doi.org/10.1016/j.enconman.2023.117545.

Wang, H., Long, X., Cao, X., Li, L., Zhang, J., Zhao, Y., Wang, D., Wang, Z., Meng, H., Dong, W., Jiang, C., Li, J., Li, X., (2023). Stimulation of atrazine degradation by activated carbon and cathodic effect in soil microbial fuel cell. Chemosphere 320, 138087. https://doi.org/10.1016/j.chemosphere.2023.138087.

Wu, C., Song, X., Wang, D., Ma, Y., Ren, X., Hu, H., Shan, Y., Ma, X., Cui, J., Ma, Y., (2023). Effects of long-term microplastic pollution on soil heavy metals and metal resistance genes: Distribution patterns and synergistic effects. Ecotoxicology and Environmental Safety 262, 115180. https://doi.org/10.1016/j.ecoenv.2023.115180.

Wu, Y., Wen, Q., Chen, Z., Fu, Q., Bao, H., (2022). Response of antibiotic resistance to the co-exposure of sulfamethoxazole and copper during swine manure composting. Science of The Total Environment 805, 150086. https://doi.org/10.1016/j.scitotenv.2021.150086.

Yoon, Y., Kim, B., Cho, M., (2023). Mineral transformation of poorly crystalline ferrihydrite to hematite and goethite facilitated by an acclimated microbial consortium in electrodes of soil microbial fuel cells. Science of The Total Environment 902, 166414. https://doi.org/10.1016/j.scitotenv.2023.166414.

Youssef, Y.A., Abuarab, M.E., Mahrous, A., Mahmoud, M., (2023). Enhanced degradation of ibuprofen in an integrated constructed wetland-microbial fuel cell: treatment efficiency, electrochemical characterization, and microbial community dynamics. RSC Advances 13(43), 29809-29818. https://doi.org/10.1039/D3RA05729A.

Yu, B., Feng, L., He, Y., Yang, L., Xun, Y., (2021). Effects of anode materials on the performance and anode microbial community of soil microbial fuel cell. Journal of Hazardous Materials 401, 123394. https://doi.org/10.1016/j.jhazmat.2020.123394.

Yu, B., Tian, J., Feng, L., (2017). Remediation of PAH polluted soils using a soil microbial fuel cell: Influence of electrode interval and role of microbial community. Journal of Hazardous Materials 336, 110-118. https://doi.org/10.1016/j.jhazmat.2017.04.066.

Zhang, C., Lu, H., Wang, B., Hu, Z., (2024). Study on the Performance of Two-

Compartment Microbial Fuel Cells Under Different Heavy Metal Concentrations. Water, Air, & Soil Pollution 235(1), 58. https://doi.org/10.1007/s11270-023-06869-6.

Zhang, G., Wang, Z., Liu, M., Huang, L., Jiao, Y., Zhao, Z., (2023a). Self-Driven Electrokinetic Remediation of Cd Contamination Soil by Using Double-Chamber Microbial Fuel Cell. Journal of The Electrochemical Society 170(7), 075502. https://doi.org/10.1149/1945-7111/ace6fd.

Zhang, Q., Wang, L., Xu, D., Tao, Z., Li, J., Chen, Y., Cheng, Z., Tang, X., Wang, S., (2023b). Accelerated Pb(II) removal and concurrent bioelectricity production via constructed wetland-microbial fuel cell: Structural orthogonal optimization and microbial response mechanism. Journal of Water Process Engineering 56, 104287. https://doi.org/10.1016/j.jwpe.2023.104287.

Zhao, S., Li, H., Zhou, J., Sumpradit, T., Salama, E.-S., Li, X., Qu, J., (2024). Simultaneous degradation of NSAIDs in aqueous and sludge stages by an electron-Fenton system derived from sediment microbial fuel cell based on a novel Fe@Mn biochar GDC. Chemical Engineering Journal 482, 148979. https://doi.org/10.1016/j.cej.2024.148979.